Supplementary information

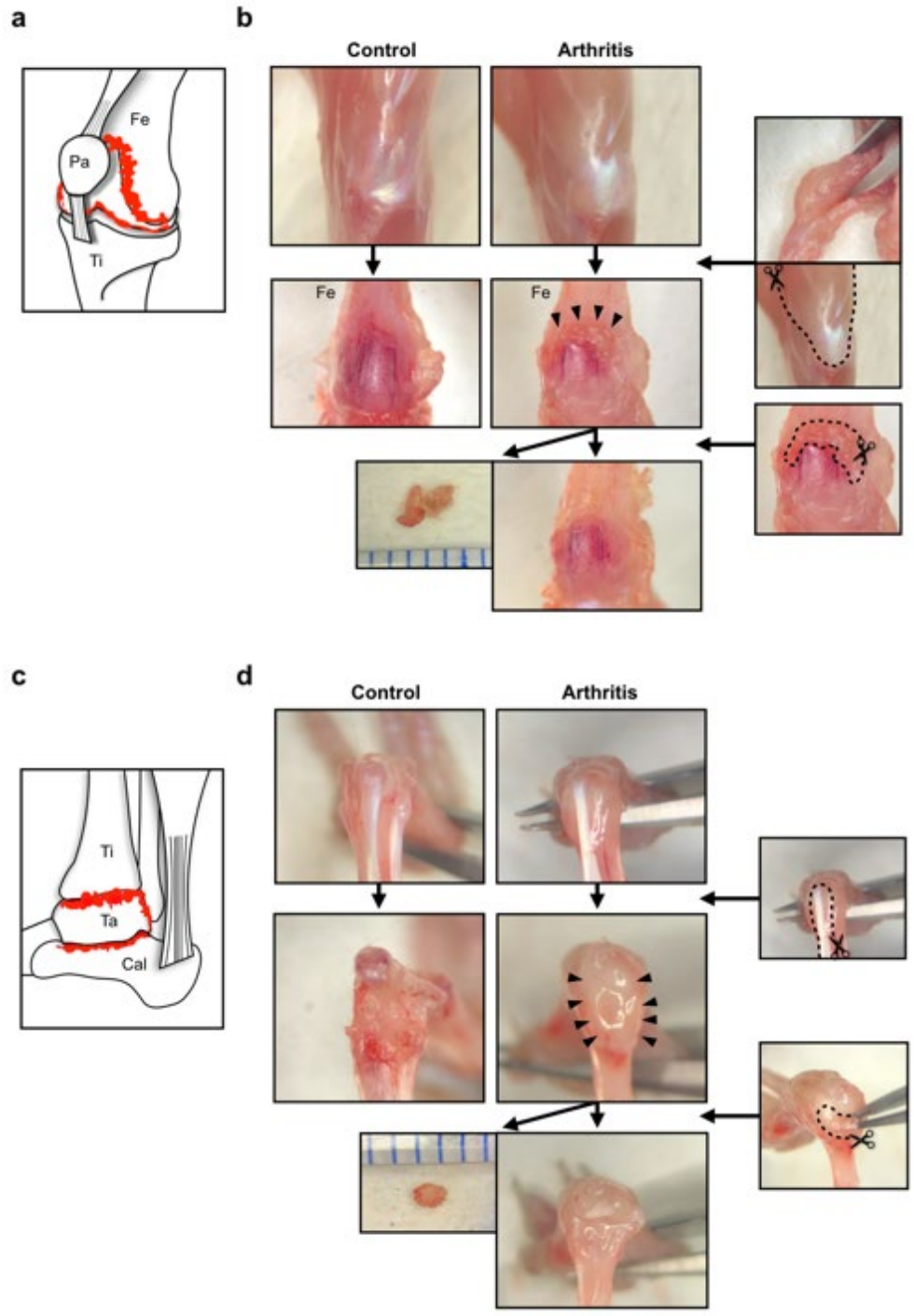

Supplementary Figure 1. Protocol for isolating pannus (hypertrophied synovium) in arthritic mice

a, Schematic diagram showing that hypertrophied synovium exists behind the patellar ligament and on the “bare area” of the femur, where bone is exposed to the synovium without a cartilage covering. Pa; patella, Fe; femur, Ti; tibia. The red lesion indicates the hypertrophied synovium on the bare area.

b, After removal of the biceps femoris muscle, the quadriceps femoris muscles including the vastus intermedius muscle were pinched and lifted with tweezers. The quadriceps femoris muscles and patellar ligament, including the patella, were isolated from the knee joint under a stereoscopic microscope. The hypertrophied synovium is visible on bare areas of the femur (arrowheads) and isolated without damaging the bone.

c, Schematic diagram showing that hypertrophied synovium exists behind the Achilles tendon. Ti; Tibia, Ta; Talus, Cal; Calcaneus. The red lesion indicates the hypertrophied synovium.

d, After removal of the ankle joint tendons, including the Achilles tendon, the hypertrophied synovium can be detected around the talus (arrowheads) and isolated without damaging the bone.

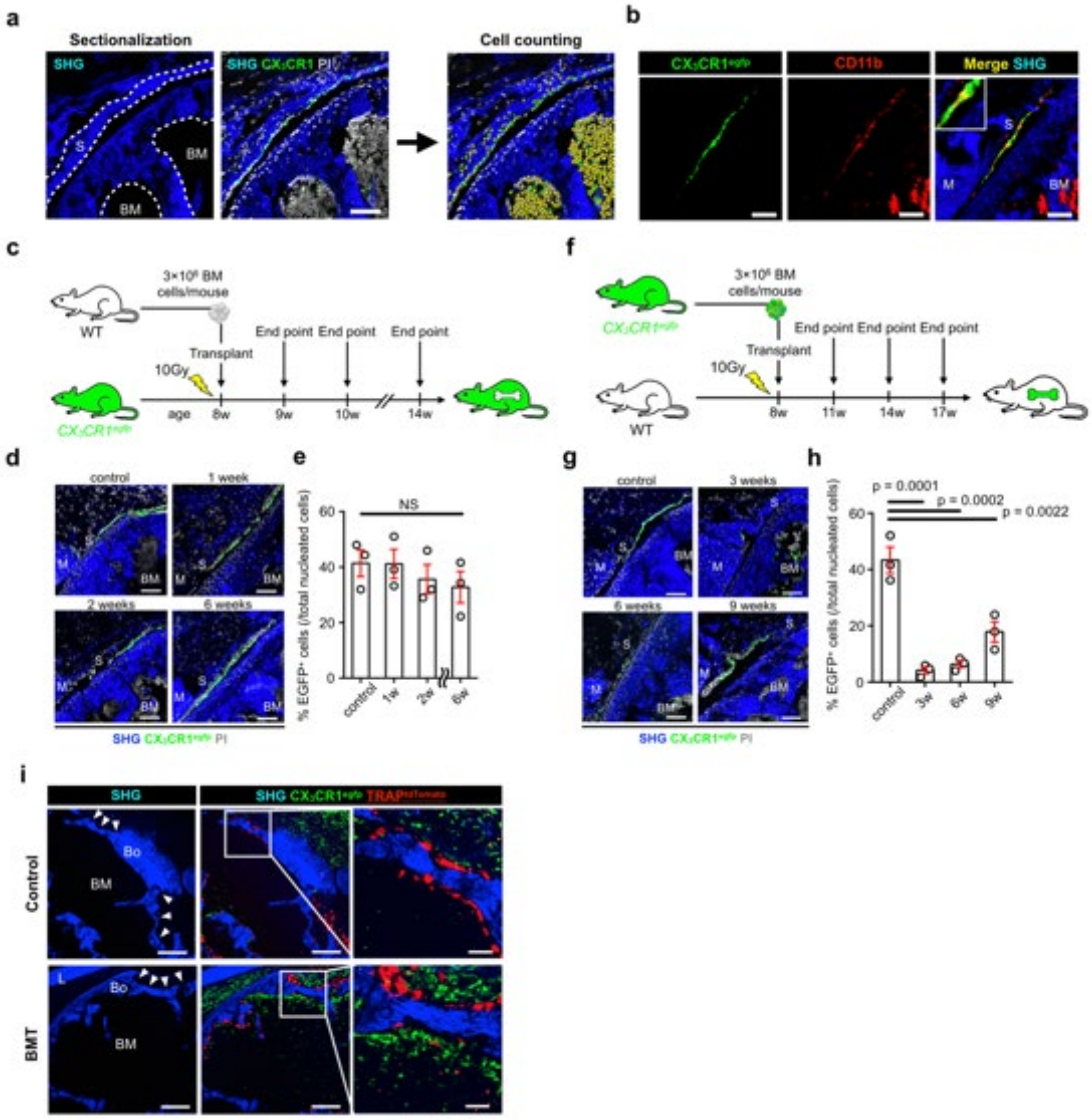

Supplementary Figure 2. CX_3CR1-EGFP$^+$ resident macrophages are radio-resistant and slowly replaced by bone marrow cells (related to Fig. 1).

a, Sectionalization of synovium (S) and bone marrow (BM) using second harmonic generation (SHG) and cell counting by Imaris software. Bar, 70 μm.

b, Immunohistochemistry of CX_3CR1-EGFP transgenic mice healthy knee joints stained with Ab against CD11b (BV421). Bars, 70 μm.

c, Schematic diagram showing the experimental design for production of bone marrow chimeric mice with wild-type hematopoietic cells.

d, Representative confocal images of knee joints showing recipient-derived $EGFP^+$ macrophages in the synovium (S) attached to the meniscus (M) with PI and SHG at multiple time points post-transplantation. Bars, 70 μm.

e, Quantification of recipient-derived $EGFP^+$ cells in the synovium as percentages of total nucleated cells at the indicated time points following BM transplantation. Symbols represent individual mice.

f, Schematic diagram showing the experimental design for the production of bone marrow chimeric mice with CX_3CR1-EGFP transgenic hematopoietic cells.

g, Representative confocal images of knee joints showing donor-derived $EGFP^+$ macrophages in the synovium (S) attached to the meniscus (M). Bars, 70 μm.

h, Quantification of donor-derived $EGFP^+$ cells in the synovium as percentages of total nucleated cells at the indicated time points following bone marrow transplantation.

i, Representative confocal images of CX_3CR1-$EGFP^+$ cells and TRAP-$tdTomato^+$ osteoclasts in arthritic knee joints of double transgenic mice (Control) and bone marrow chimeric mice (BMT). Bo: bone, L: patellar ligament. Arrowheads indicate bone erosion. Bars, 200 and 50 μm.

One-way ANOVA with Bonferroni's post hoc test (e, h). Mean ± S.E.M. for each group. Symbols represent individual mice.

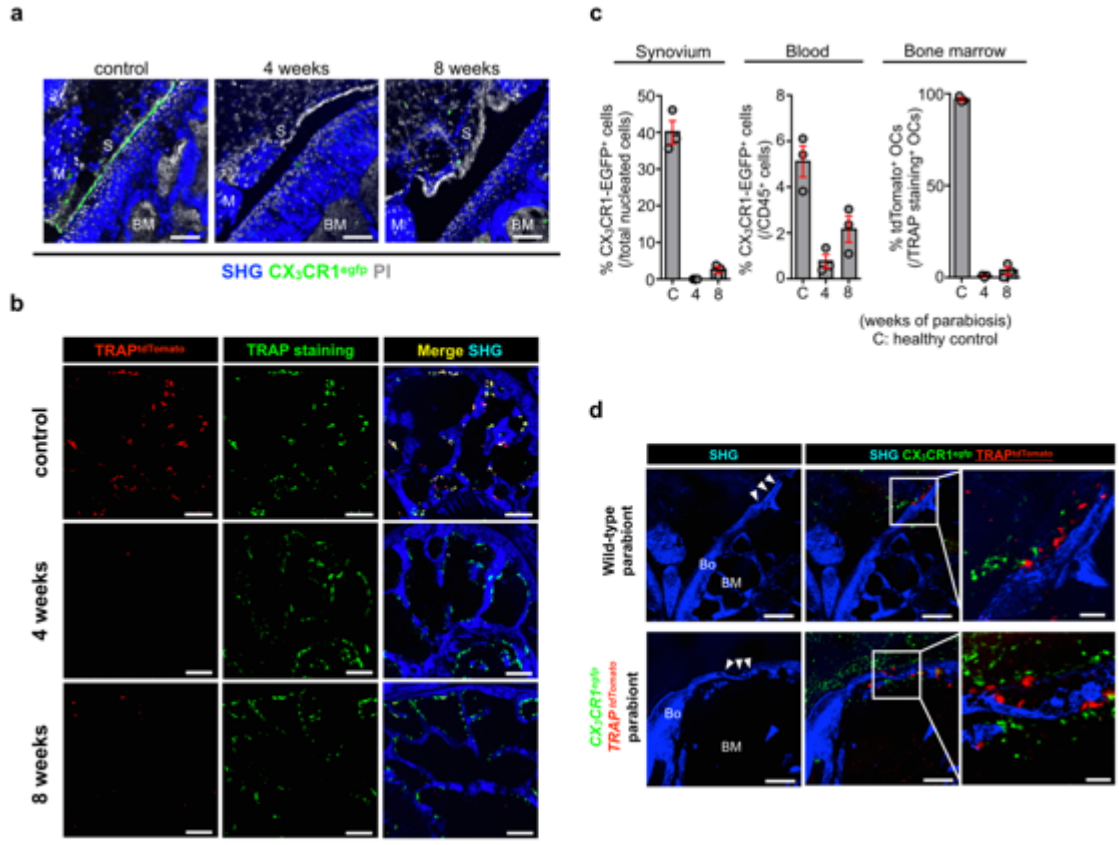

Supplementary Figure 3. Wild-type and double transgenic mice (CX$_3$CR1-EGFP/TRAP-tdTomato) analyzed at 4 or 8 weeks of parabiosis (related to Fig. 1).

a, Representative confocal images of CX$_3$CR1-EGFP$^+$ cells in the synovium (S) attached to the meniscus (M) with PI and SHG in CX$_3$CR1-EGFP transgenic mice (control) and wild-type parabionts at the indicated time points. Bars, 70 µm.

b, Representative confocal images of TRAP-tdTomato$^+$ osteoclasts and TRAP staining$^+$ osteoclasts in bone marrow. Bars, 150 µm.

c, Histograms represent percentages of CX_3CR1-EGFP and TRAP-tdTomato$^+$ cells in the synovium, blood, and bone marrow of wild-type parabionts. Quantification of CX_3CR1-EGFP$^+$ cells in blood was conducted by FACS. Mean ± S.E.M. for each group. Symbols represent individual mice.

d, Representative confocal images of CX_3CR1-EGFP$^+$ cells and TRAP-tdTomato$^+$ osteoclasts in arthritic knee joints from indicated parabionts. Bars, 200 and 50 μm.

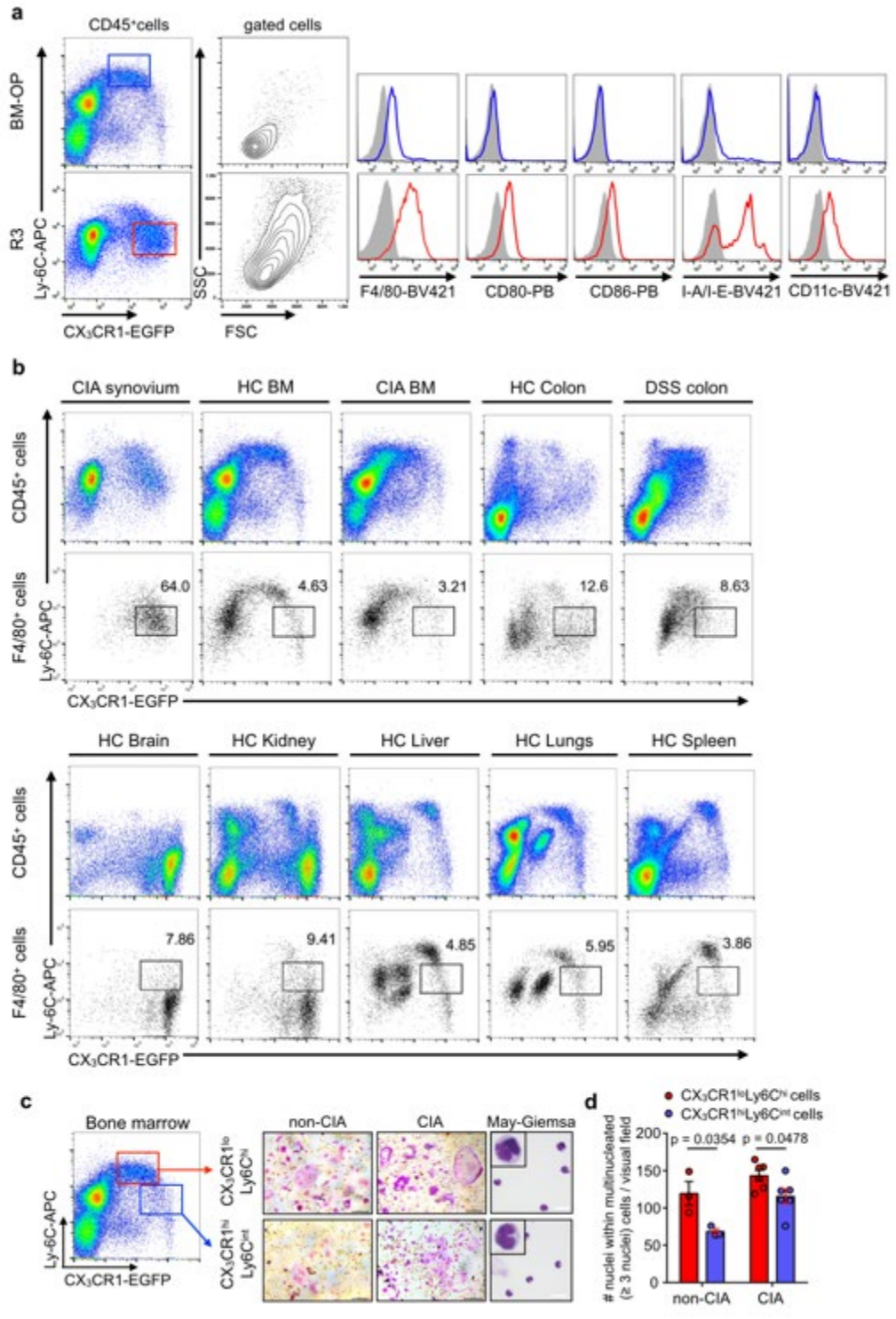

Supplementary Figure 4. Comparison of CD45$^+$F4/80$^+$ cells in synovium and other organs.

a, Phenotypic marker comparison of conventional OP-containing population in bone marrow (BM-OP; $CX_3CR1^{lo}Ly6C^{hi}$ cells) and R3 cells in the inflamed synovium.

b, Representative plots of $CD45^+F4/80^+$ cells from various of organs of CX_3CR1-EGFP transgenic mice.

c, Representative TRAP staining images of RANKL-induced osteoclastogenesis and May-Giemsa staining of $CX_3CR1^{lo}Ly6C^{hi}$ cells and $CX_3CR1^{hi}Ly6C^{int}$ cells from BM in CIA and non-CIA mice. Bars, 200 and 20 μm.

d, Quantification of nuclei in multinucleated cells within the visual field in **c**.

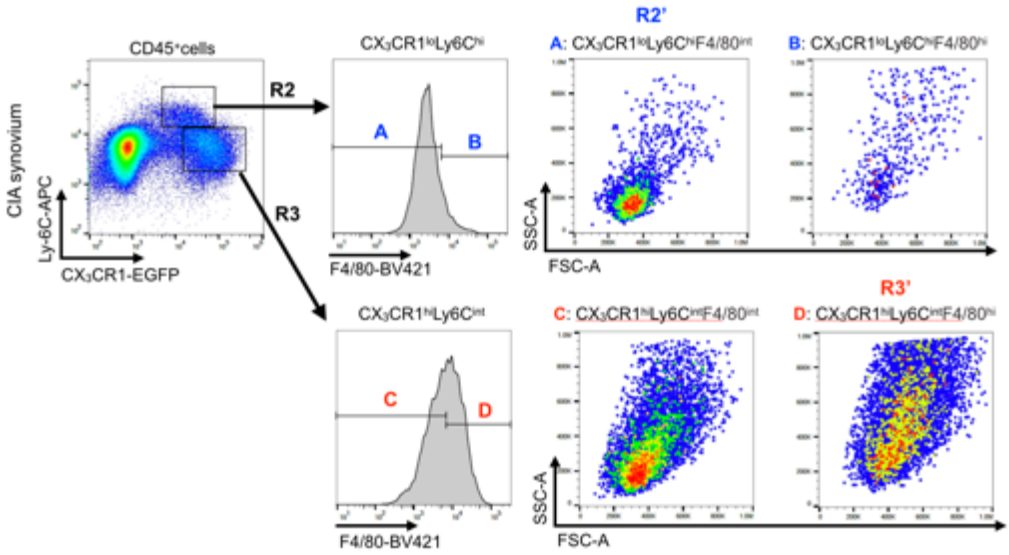

Supplementary Figure 5. Definition of R2' and R3' fractions based on the expression level of F4/80.

Both R2 and R3 fractions may contain transitional states. R2 ($CX_3CR1^{lo}Ly6C^{hi}$) and R3 ($CX_3CR1^{hi}Ly6C^{int}$) cells in the inflamed synovium were further gated on F4/80 to discriminate transitional status and to define R2' ($CX_3CR1^{lo}Ly6C^{hi}F4/80^{int}$) and R3' ($CX_3CR1^{hi}Ly6C^{int}F4/80^{hi}$), respectively. R3' is defined as "fully differentiated R3", and R2' is defined as "basal state R2".

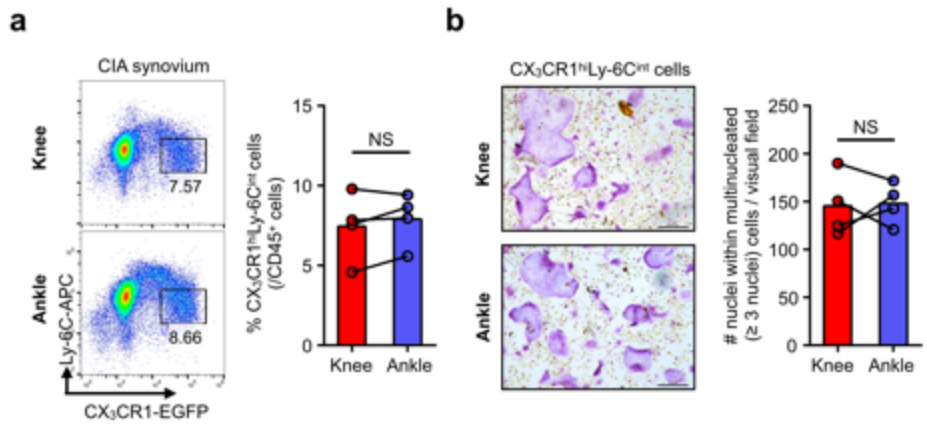

Supplementary Figure 6. Comparison of R3 cells in knee and ankle joints from CIA mice.

a, Representative plots and quantitative data of $CX_3CR1^{hi}Ly6C^{int}$ cells (R3) in the knee and ankle joints from CIA mice one week after arthritis onset.

b, Representative TRAP staining images and quantification of nuclei in multinucleated cells of RANKL-induced osteoclastogenesis of R3 cells in the knee and ankle joints from CIA mice. Bars, 200 μm.

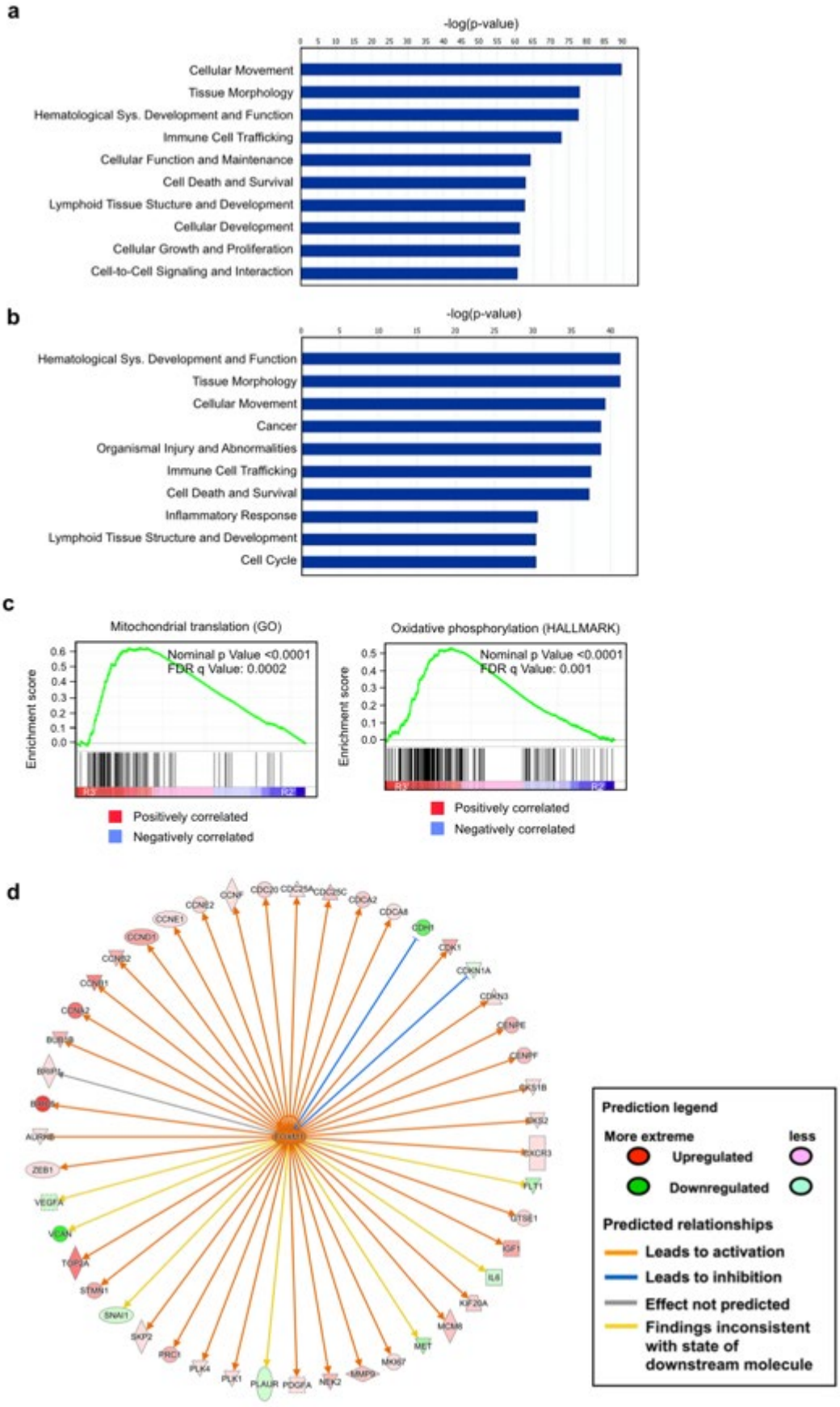
a
-log(p-value)
Cellular Movement
Tissue Morphology
Hematological Sys. Development and Function
Immune Cell Trafficking
Cellular Function and Maintenance
Cell Death and Survival
Lymphoid Tissue Stucture and Development
Cellular Development
Cellular Growth and Proliferation
Cell-to-Cell Signaling and Interaction
b
-log(p-value)
Hematological Sys. Development and Function
Tissue Morphology
Cellular Movement
Cancer
Organismal Injury and Abnormalities
Immune Cell Trafficking
Cell Death and Survival
Inflammatory Response
Lymphoid Tissue Structure and Development
Cell Cycle
c
Mitochondrial translation (GO)
Nominal p Value <0.0001
FDR q Value: 0.0002
Enrichment score
Positively correlated
Negatively correlated
Oxidative phosphorylation (HALLMARK)
Nominal p Value <0.0001
FDR q Value: 0.001
Enrichment score
Positively correlated
Negatively correlated
d
Prediction legend
More extreme
less
Upregulated
Downregulated
Predicted relationships
Leads to activation
Leads to inhibition
Effect not predicted
Findings inconsistent with state of downstream molecule

1

Supplementary Figure 7. Transcriptional profiling of R1, R2', and R3' cells by RNA-Seq (related to Fig. 4).

a, Downstream effects analysis of R2'/R1 cells and **b,** R3'/R2' cells by RNA-Seq.

c, Enrichment analysis of mitochondrial translation and oxidative phosphorylation in R3' cells compared with R2' cells.

d, Upstream analysis of FoxM1 in R3'/R2' cells by RNA-Seq.

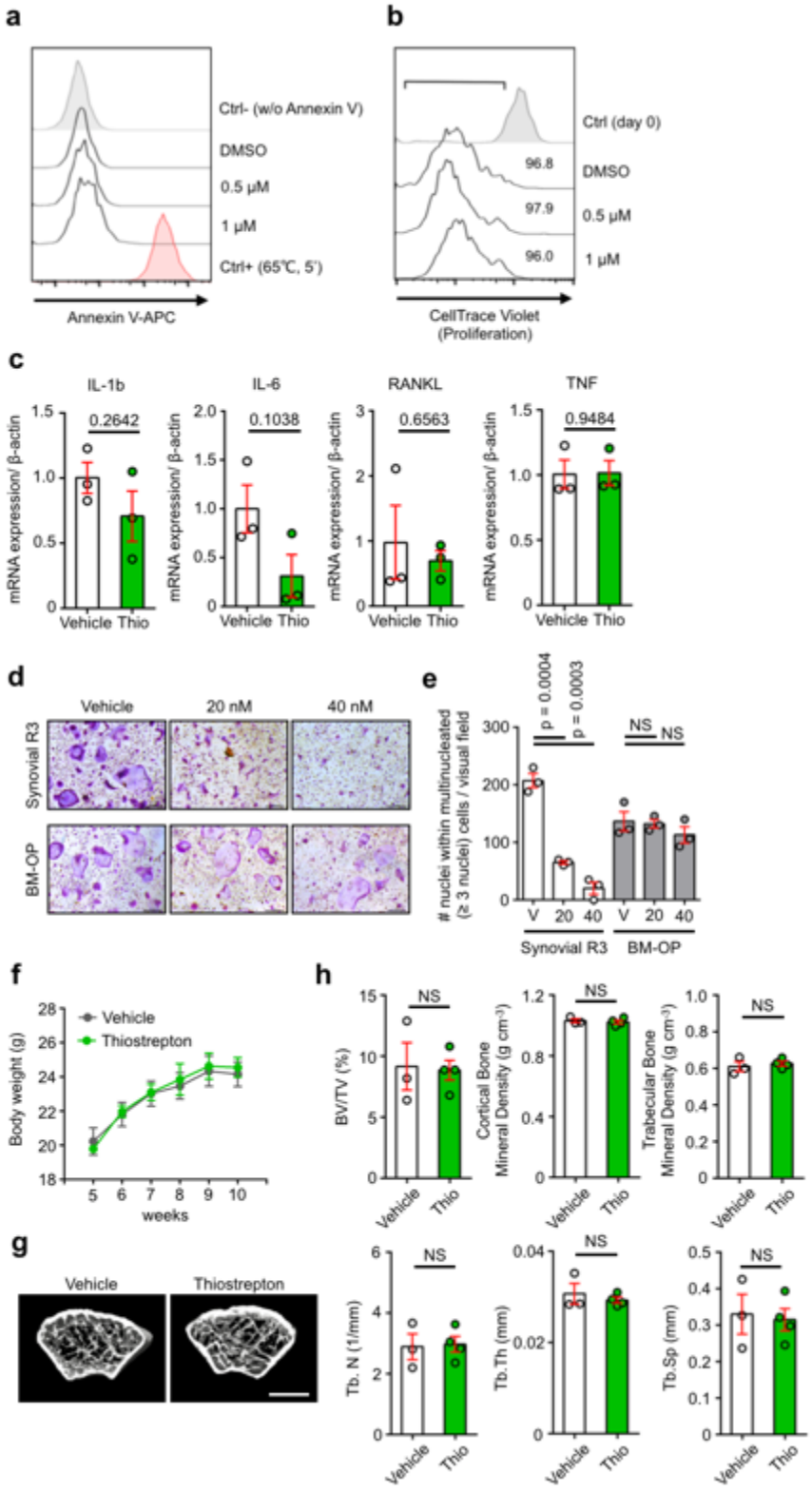

Supplementary Figure 8. Effects of thiostrepton *in vitro* and *in vivo* (related

to Fig. 4).

a, Histogram plots of annexin-V positive bone marrow macrophages treated with 10 ng/ml M-CSF and DMSO or thiostrepton for 48 hours.

b, Histogram plots displaying proliferation of bone marrow macrophages treated with 10 ng/ml M-CSF and DMSO or thiostrepton for 48 hours, determined by CellTrace Violet signal.

c, RT-PCR analysis of IL-1, IL-6, RANKL, and TNF expression in synovial tissues from CIA mice treated with vehicle or 50 mg/kg thiostrepton. Vehicle or thiostrepton were injected intraperitoneally every other day for 2 weeks before sacrifice.

d, Representative TRAP staining images of RANKL-induced osteoclastogenesis of synovial $CX_3CR1^{hi}Ly6C^{int}$ cells (R3 cells) and $CX_3CR1^{lo}Ly6C^{hi}$ cells from BM (BM-OP) treated with thiostrepton.

e, Quantification of nuclei in multinucleated cells within the visual field depicted in **d**. Bars, 200 μm.

f, Body weight of WT mice treated with vehicle or 50 mg/kg thiostrepton from 5

weeks to 10 weeks of age. Vehicle or thiostrepton were injected intraperitoneally twice a week for 5 weeks.

g, Axial view of femur metaphyseal region in 10-week-old mice treated with vehicle or thiostrepton as described in **f** . Bar, 1 mm.

h, Quantification results of micro CT analysis; bone volume/total volume (BV/TV), cortical bone mineral density, trabecular bone mineral density, trabecular number (Tb.N), trabecular thickness (Tb.Th), and trabecular space (Tb.Sp) were measured.

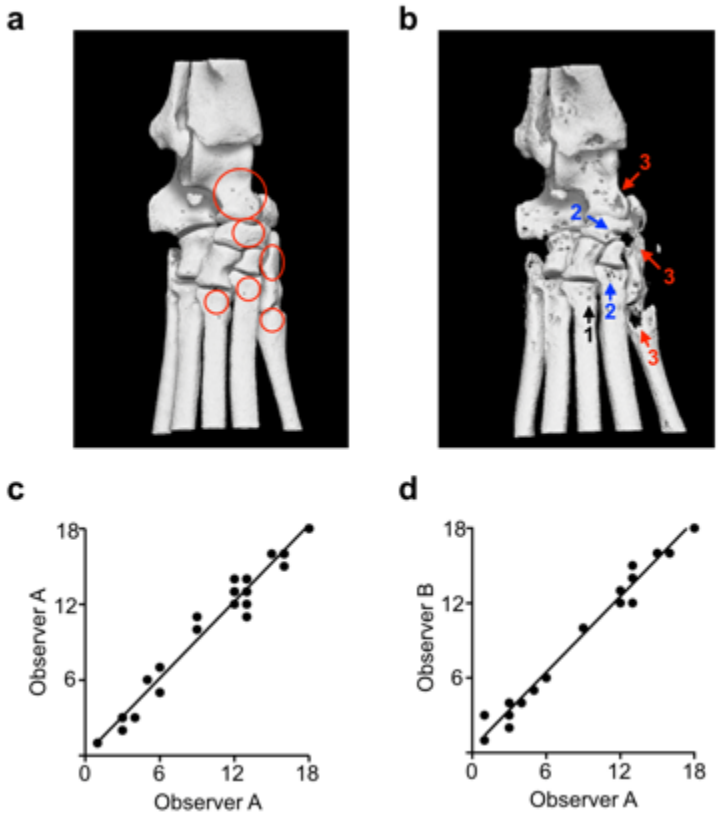

Supplementary Figure 9. A semi-quantitative scoring method for hind paw erosion on micro-CT (related to Figs. 4, 7).

a, 3D reconstructions of hind paws were scored at six anatomical sites: talus, navicular bone, medial cuneiform bone, and the bases of the first, second, and third metatarsals.

b, Erosions were scored on a scale of 0–3 (0 = normal, 1 = pitting, 2 = full-thickness holes in small–medium areas, 3 = full-thickness holes in medium–large areas) with a maximum score of 18.

c–d, Intra-observer and inter-observer reproducibility were r = 0.9831 and 0.9883, respectively. Scatter dots represent individual mice.

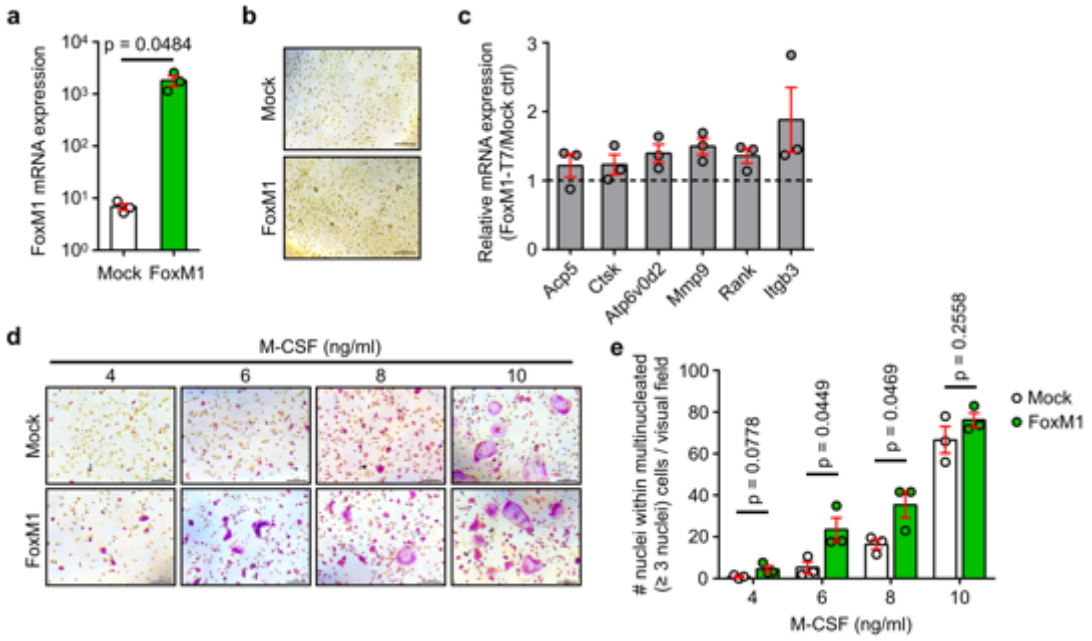

Supplementary Figure 10. Overexpression of FoxM1 partially replaces the M-CSF contribution to osteoclastogenesis.

a, RT-PCR analysis of FoxM1 expression in bone marrow macrophages electroporated with CMV-T7-FoxM1 plasmid or mock plasmid.

b, Representative TRAP staining images of macrophages electroporated with CMV-T7-FoxM1 plasmid or mock plasmid without RANKL stimulation.

c, RT-PCR analysis of osteoclast marker gene expression in bone marrow macrophages electroporated with CMV-T7-FoxM1 plasmid or mock plasmid without RANKL stimulation. The ratio of expression (CMV-T7-FoxM1/Mock) is shown for each experiment.

d. Representative TRAP staining images of bone marrow macrophages electroporated with CMV-T7-FoxM1 plasmid or mock plasmid. Cells were cultured with 100 ng/ml RANKL and M-CSF at the indicated concentrations. Bars, 200 μm. **e**, Quantification of nuclei within multinucleated cells within the visual field in **d**. Unpaired two-tailed *t* test (a, e). Mean ± S.E.M. for each group. Symbols represent individual mice.

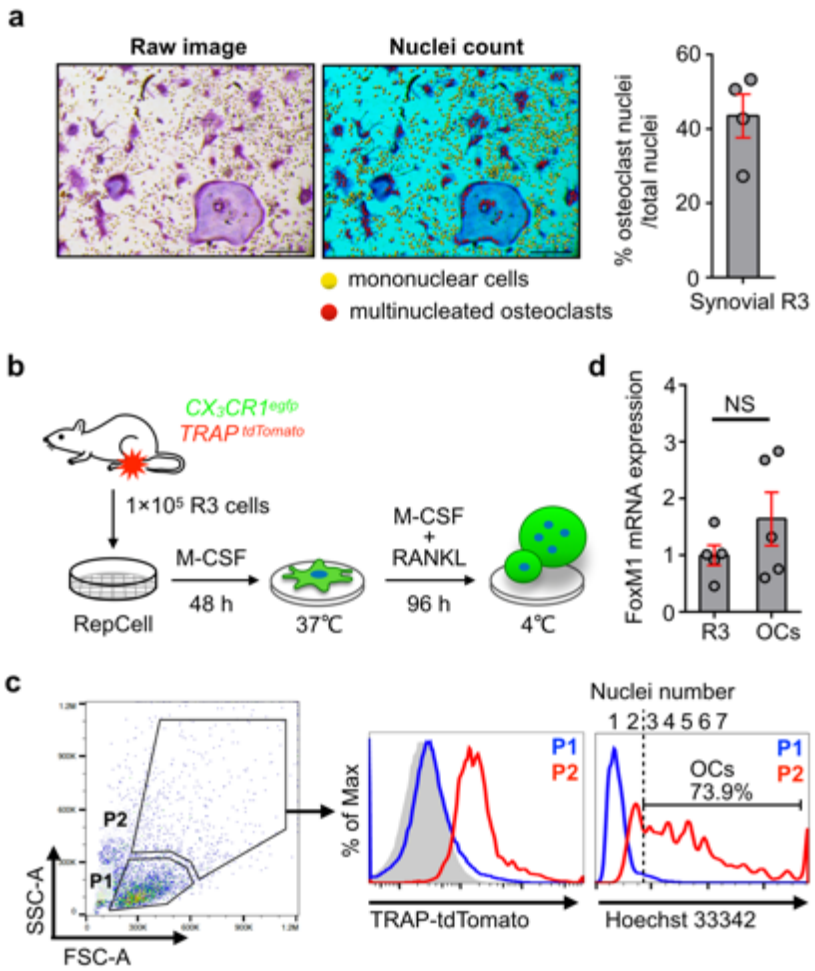

Supplementary Figure 11. Isolation of mature osteoclasts differentiated from R3 cells.

a, Representative TRAP staining images of RANKL-induced osteoclastogenesis of synovial $CX_3CR1^{hi}Ly6C^{int}$ cells (R3 cells) and nuclei quantification of mononuclear cells and multinucleated mature osteoclasts using Imaris software. Bars, 200 μm.

b, Schematic diagram depicting the procedure for isolation of mononuclear cells and multinucleated mature osteoclasts using temperature-responsive cell cultureware, RepCell.

c, Representative plots of isolated cells from RepCell. $FSC^{lo}SSC^{lo}$ population (P1) and $FSC^{hi}SSC^{hi}$ population (P2) were analyzed for TRAP-tdTomato and Hoechst 33342. $FSC^{hi}SSC^{hi}tdTomato^{+}$ population with multiple nuclei were gated as mature osteoclasts. Shaded region indicates control values from wild-type mice.

d, RT-PCR analysis of FoxM1 expression in R3 cells and resultant osteoclasts. Unpaired two-tailed *t* test (d). Mean ± S.E.M. for each group. Symbols represent individual mice in **a** and a single experiment in **d**.

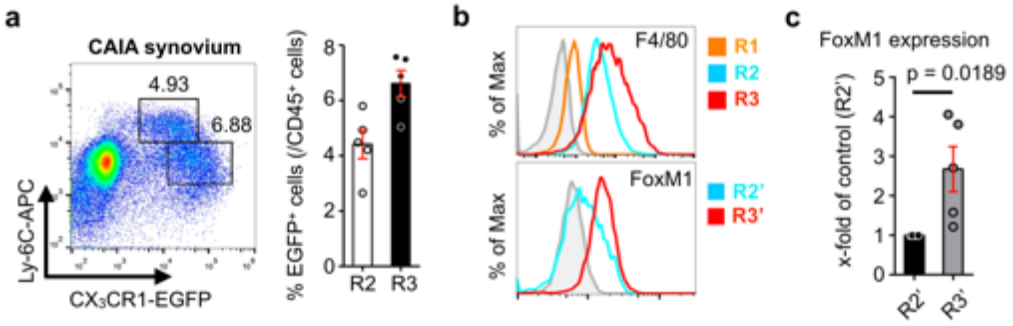

Supplementary Figure 12. Presence of $CX_3CR1^{hi}Ly6C^{int}F4/80^{hi}$ macrophages (R3' cells) in the inflamed synovium of collagen antibody-induced arthritis (CAIA) model (related to Fig. 7).

a, Representative plots and quantitative data of CX_3CR1-$EGFP^+$ cells in the inflamed knee synovium of CAIA mice.

b, Phenotypic characterization of R1, R2 (R2'), and R3 (R3') cells by FACS. Shaded regions indicate staining with isotype controls.

c, RT-PCR analysis of FoxM1 expression in R2' cells and R3' cells.

Unpaired two-tailed *t* test (c). Mean ± S.E.M. for each group. Symbols represent individual mice.

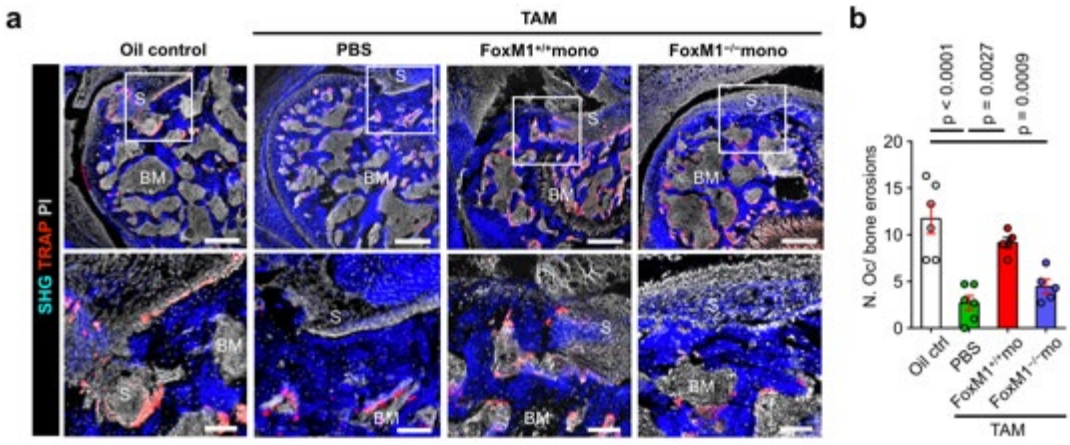

Supplementary Figure 13. Histological examination of inflamed knee joints in FoxM1$^{fl/fl}$ Rosa26^{CreERT2} mice (related to Fig. 7).

a, Histological examination of knee joints from CAIA mice treated with oil control, tamoxifen, tamoxifen plus adoptive transfer of FoxM1$^{+/+}$CX$_3$CR1$^+$ monocytes or FoxM1$^{-/-}$CX$_3$CR1$^+$monocytes. BM: bone marrow; S: synovium. Bars, 300 and 100 μm.

b, Number of osteoclasts (N. Oc) per visual field at the sites of bone erosions. Symbols represent individual mice and values represent the average count of three different sections.

One-way ANOVA with Bonferroni's post hoc test. Mean ± S.E.M. for each group.

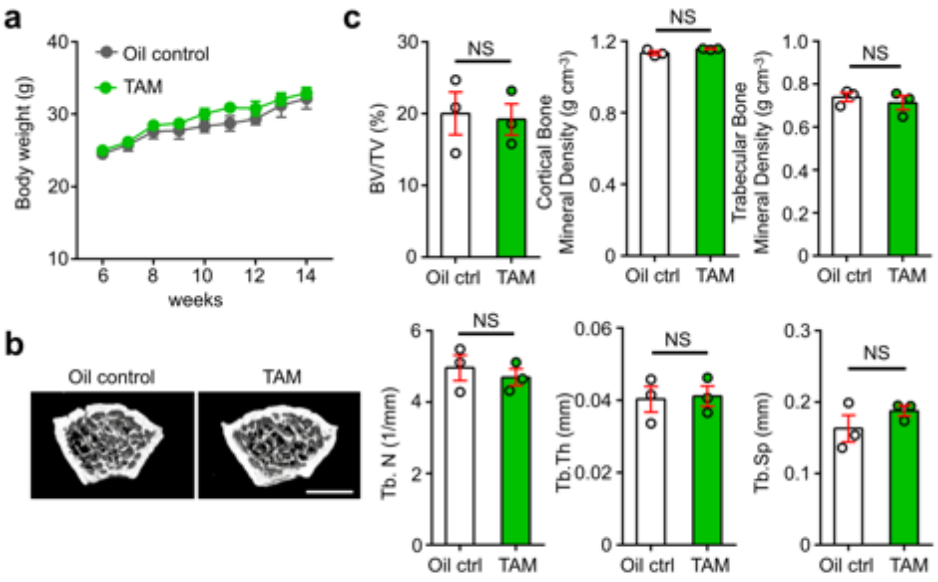

Supplementary Figure 14. Physiological bone remodelling was not affected by global FoxM1 deletion.

a, Body weight of FoxM1$^{fl/fl}$Rosa26^{CreERT2} mice treated with oil control or tamoxifen from 6 weeks of age; 2 mg tamoxifen was injected intraperitoneally 3 days in a row from 6 weeks of age, and was repeated from 10 weeks of age.

b, Axial view of the femur metaphyseal region of 14-week-old FoxM1$^{fl/fl}$Rosa26^{CreERT2} mice treated with oil control or tamoxifen. Bar, 1 mm.

c, Quantification of the micro CT analysis: bone volume/total volume (BV/TV), cortical bone mineral density, trabecular bone mineral density, trabecular number (Tb.N), trabecular thickness (Tb.Th), and trabecular space (Tb.Sp) were

measured in the femur metaphyseal region of 14-week-old FoxM1$^{fl/fl}$Rosa26^{CreERT2} mice treated with oil control or tamoxifen.

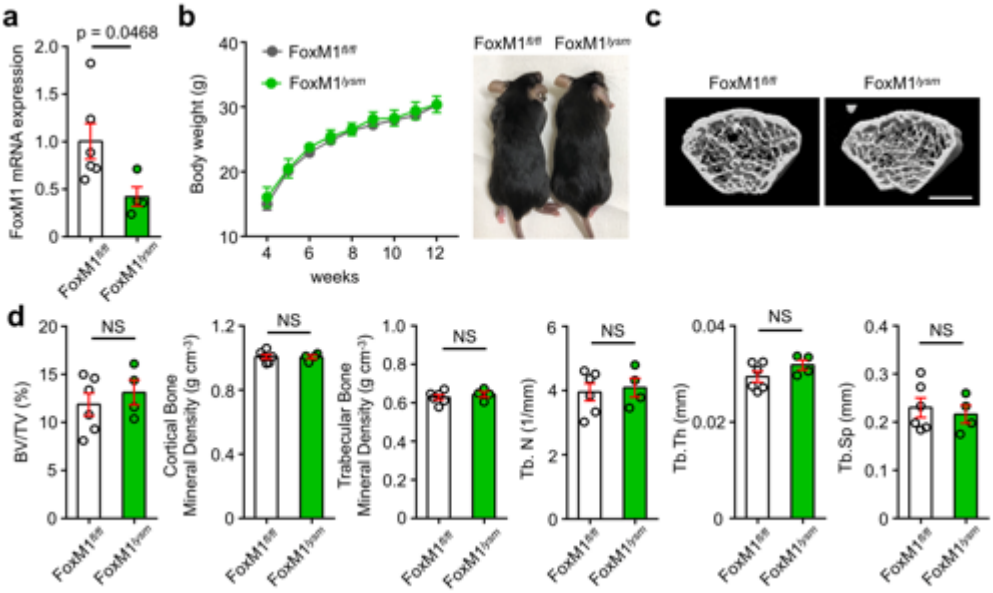

Supplementary Figure 15. Physiological bone remodelling was not affected in LysM-Cre:FoxM1$^{fl/fl}$ mice.

a, RT-PCR analysis of FoxM1 expression in $CX_3CR1^{+}Ly6C^{hi}$ bone marrow cells (BM-OP) from FoxM1$^{fl/fl}$ and LysM-Cre;FoxM1$^{fl/fl}$ mice.

b, Body weight of FoxM1$^{fl/fl}$ and LysM-Cre:FoxM1$^{fl/fl}$ mice.

c, Axial view of the femur metaphyseal region of 8-week-old FoxM1$^{fl/fl}$ and LysM-Cre:FoxM1$^{fl/fl}$ mice. Bar, 1 mm.

d, Quantification results of micro CT analysis; bone volume/total volume (BV/TV), cortical bone mineral density, trabecular bone mineral density, trabecular number (Tb.N), trabecular thickness (Tb.Th), and trabecular space (Tb.Sp) were

measured in the femur metaphyseal region of 8-week-old FoxM1$^{fl/fl}$ and LysM-Cre:FoxM1$^{fl/fl}$ mice.

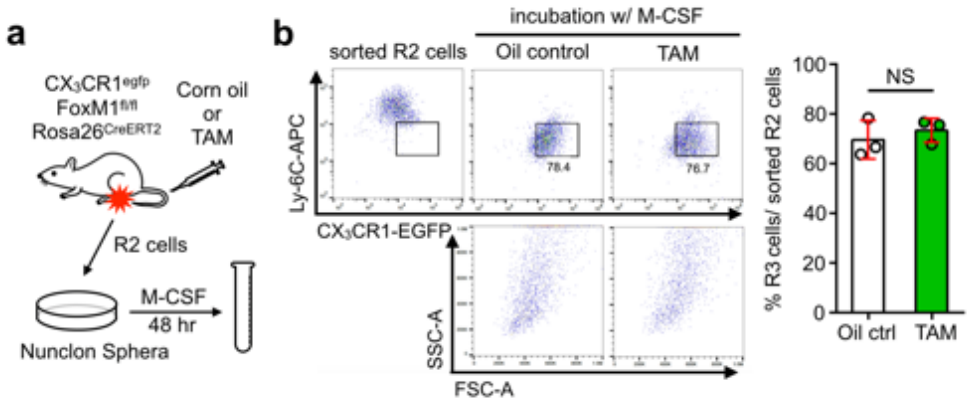

Supplementary Figure 16. FoxM1 is dispensable for R2 to R3 cell differentiation.

a, Schematic diagram showing that synovial R2 cells from CAIA mice treated with corn oil or tamoxifen were sorted into Nunclon Sphere plates and incubated for 48 hours with 10 ng/ml M-CSF.

b, Flow cytometry plots of R2 cells incubated with 10 ng/ml M-CSF and percentage of resultant $CX_3CR1^{hi}Ly6C^{int}$ cells (R3).

Unpaired two-tailed *t* test (b). Mean ± S.E.M. for each group. Symbols represent individual mice.

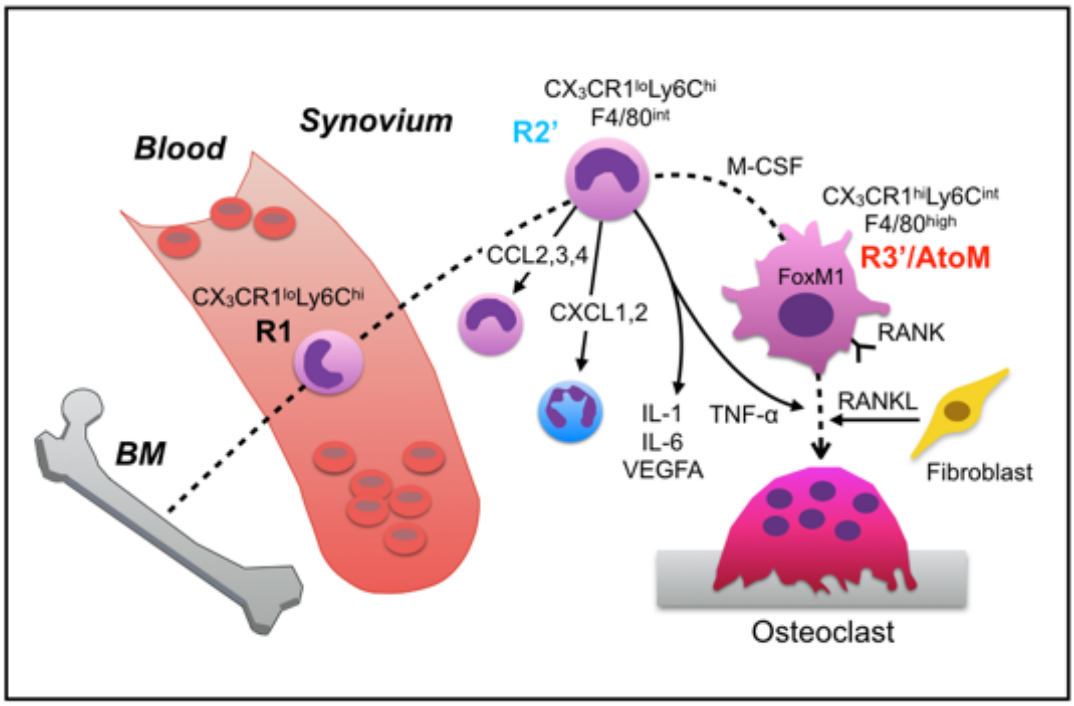

Supplementary Figure 17. Schematic diagram of the differentiation trajectory of inflammatory OPs in arthritis.

$CX_3CR1^{lo}Ly6C^{hi}$ cells in the blood (R1) trans-migrate into the synovium as $CX_3CR1^{lo}Ly6C^{hi}F4/80^{int}$ cells (R2'), which express chemokines (*Ccl2, Ccl3, Ccl4, Cxcl1, Cxcl2*), inflammatory cytokines (*Tnf, Il-1, Il-6*), and *Vegfa*. A high level of M-CSF in the inflamed synovium up-regulates FoxM1 in the R2' subset and induces differentiation into R3' cells (AtoMs), the osteoclast precursors (OPs) in arthritis. R3' cells differentiate into osteoclasts upon RANKL-stimulation in pannus to cause bone erosions.

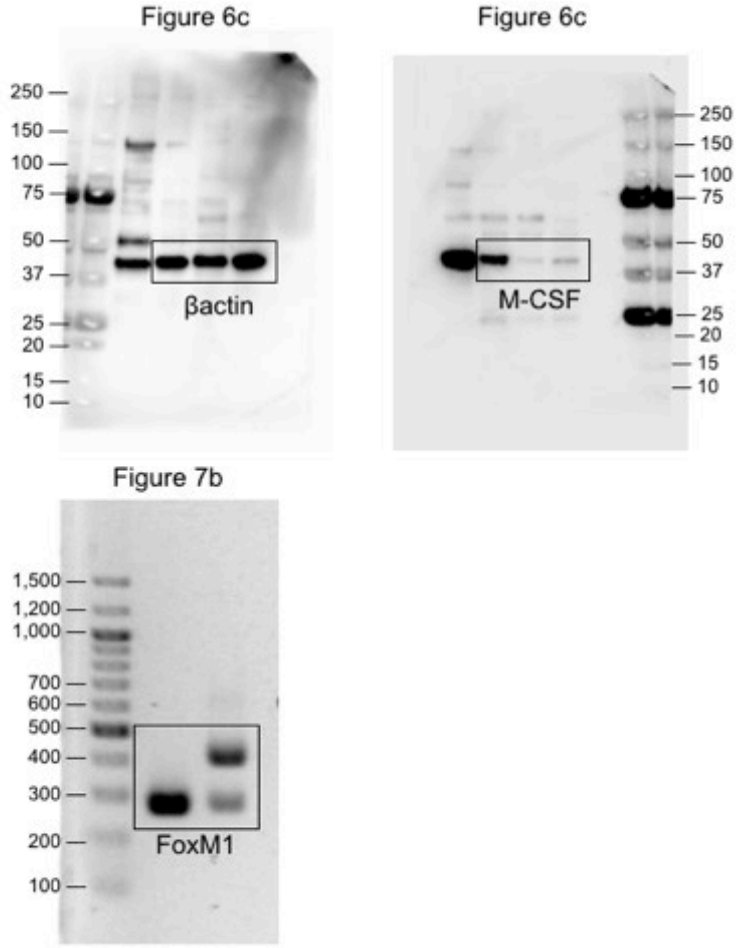

Supplementary Figure 18. Gel source data

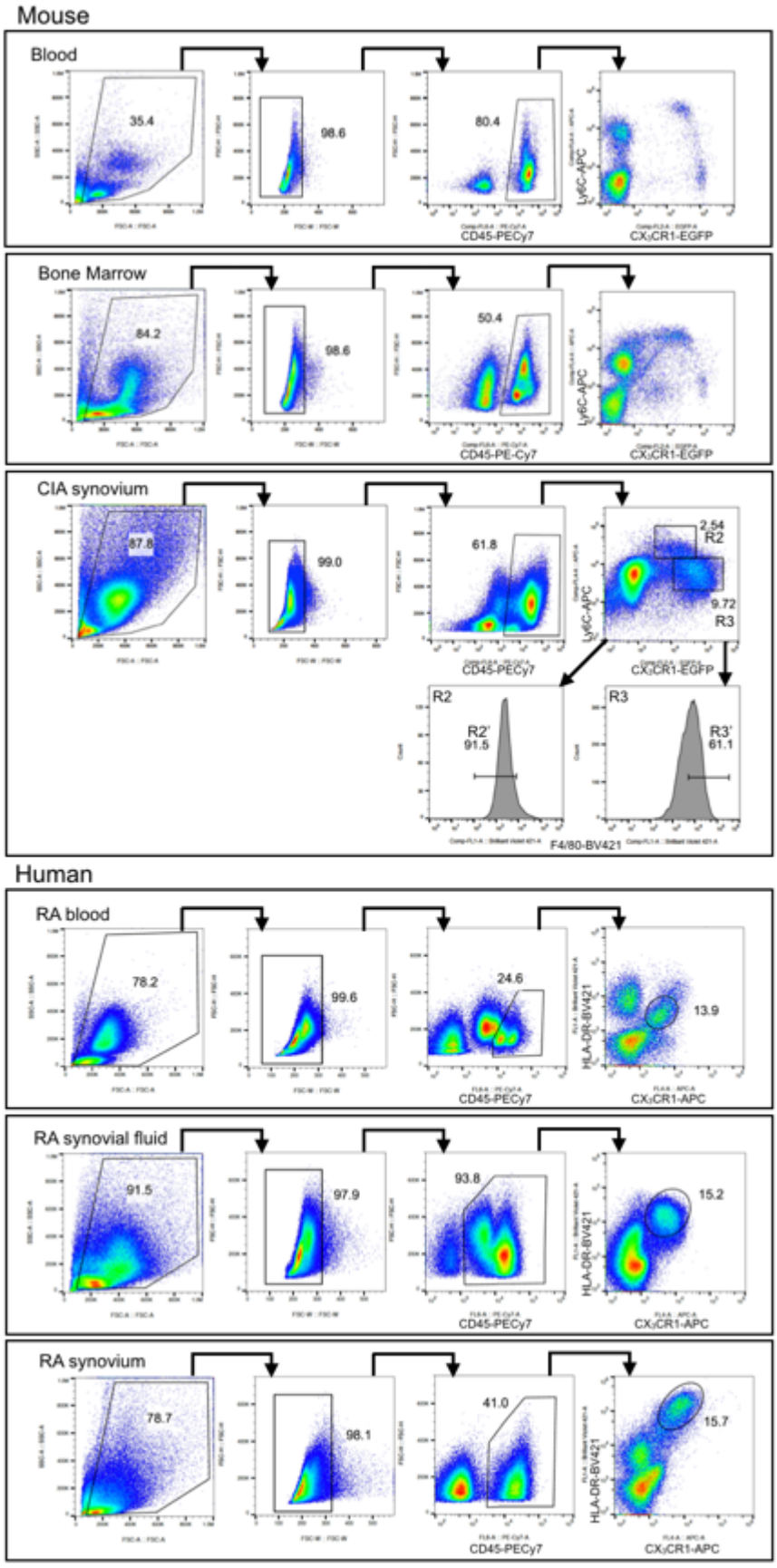
Mouse
Blood
35.4
98.6
80.4
CD45-PECy7
Ly6C-APC
CX3CR1-EGFP
Bone Marrow
84.2
98.6
50.4
CD45-PE-Cy7
Ly6C-APC
CX3CR1-EGFP
CIA synovium
87.8
99.0
61.8
2.54
R2
9.72
R3
CD45-PECy7
Ly6C-APC
CX3CR1-EGFP
R2
R2'
91.5
R3
R3'
61.1
F4/80-BV421
Human
RA blood
78.2
99.6
24.6
13.9
CD45-PECy7
HLA-DR-BV421
CX3CR1-APC
RA synovial fluid
91.5
97.9
93.8
15.2
CD45-PECy7
HLA-DR-BV421
CX3CR1-APC
RA synovium
78.7
98.1
41.0
15.7
CD45-PECy7
HLA-DR-BV421
CX3CR1-APC

1

Supplementary Figure 19. Gating strategy for different tissues.

Viable cells were enriched by scatter plots and doublet cells were excluded based on FSC-H/FSC-W. After gating on $CD45^+$ cells, R2 and R3 cells in the CIA synovium were defined according to CX_3CR1 and Ly6C. These populations were further gated by F4/80 to sort R2' and R3' cells.

Gene set		
ACP5	*FOS*	*PDGFB*
ATP6V0D2	*GLO1*	*PPARG*
CALCR	*GPC3*	*PPARGC1B*
CA2	*ITGB3*	*SEMA4D*
CD109	*JUN*	*SH3PXD2A*
CKB	*JUNB*	*SPHK1*
CSF1	*MAPK1*	*SPNS2*
CSF1R	*MAPK11*	*SRC*
CTHRC1	*MAPK12*	*TFRC*
CTNNB1	*MAPK14*	*TM7SF4*
CTSK	*MITF*	*TNFRSF11A*
C20ORF123	*MMP9*	*TNFRSF11B*
EFNA2	*NFATC1*	*TRAF2*
EFNB2	*NFKB1*	*TRAF6*
E2F1	*NFKB2*	*TREM2*
FAM20C	*OSCAR*	
FARP2	*OSTM1*	

Supplementary Table 1. Gene set related to osteoclast differentiation modified from the Broad Institute Molecular Signatures Database

Case	Diagnosis	Sex	Age	Onset of disease	Treatment	Seropositivity
1	RA	F	65	1987	MTX	RF
2	RA	F	56	2012	MTX	ACPA
3	RA	F	76	1994	MTX	RF, ACPA
4	RA	F	86	2003	PSL, Tac	RF, ACPA
5	RA	F	69	2010	MTX	RF
6	RA	F	77	2001	PSL, Tac, ADA	-
7	RA	F	89	2003	PSL, SASP, BUC, GOL	RF, ACPA
8	RA	F	67	2010	SASP	RF, ACPA
9	RA	F	76	1994	MTX, Tac	RF, ACPA
10	RA	M	87	2014	PSL, MTX, Tac	RF, ACPA
11	RA	F	58	2010	MTX	-
12	RA	F	42	2013	ADA	RF, ACPA
13	RA	F	69	1993	PSL, MTX, BOL	RF, ACPA
14	RA	F	69	2007	none	-
15	RA	M	67	1989	ETN	RF, ACPA
16	RA	F	71	1998	MTX, PSL, IGU	RF
17	RA	M	69	2003	MTX, ABT	RF, ACPA
18	RA	F	55	2018	MTX	RF, ACPA
19	RA	F	66	1992	SASP, PSL	RF, ACPA
20	RA	F	74	2018	SASP	-
21	RA	F	79	1994	Tac, TCZ	-
22	RA	F	74	2002	Tac, BUC	-
23	RA	M	54	2017	MTX, PSL	RF

Supplementary Table 2. RA patient clinical information.

MTX: methotrexate; PSL: prednisolone; Tac: tacrolimus; SASP: salazosulfapyridine; BUC: bucillamine; IGU: iguratimod; ETN: etanercept; ABT: abatacept; ADA: adalimumab; GOL: golimumab; TCZ: tocilizumab; RF: rheumatoid factor; ACPA: anti-citrullinated protein antibody.

Supplementary Video 1. *Ex vivo* incubation of inflamed synovium from double transgenic mice (CX_3CR1-EGFP/TRAP-tdTomato) (related to Fig. 1).

Harvested inflamed synovium from double transgenic mice (CX_3CR1-EGFP/TRAP-tdTomato) was incubated with 100 ng/ml RANKL and 10 ng/ml M-CSF stimulation. Sequential images of the same visual field were acquired by BioStation IM-Q (Nikon). CX_3CR1-EGFP and TRAP-tdTomato are shown as green and red, respectively, on transmission images. Playback speed is 6000X.